Title

The relationship between liver triglyceride composition and proton density fat fraction as assessed by 1H MRS

Journal

NMR in Biomedicine, 33(6)

ISSN

0952-3480

Authors

Hamilton, Gavin
Schlein, Alex N
Wolfson, Tanya
et al.

Publication Date

2020-06-01

DOI

10.1002/nbm.4286

Peer reviewed

HHS Public Access

Author manuscript

NMR Biomed. Author manuscript; available in PMC 2021 June 01.

Published in final edited form as:

NMR Biomed. 2020 June ; 33(6): e4286. doi:10.1002/nbm.4286.

The relationship between liver triglyceride composition and proton density fat fraction as assessed by ^{1}H MRS

Gavin Hamilton, PhD[1], **Alex N. Schlein, BS**[1], **Tanya Wolfson, MA**[2], **Guilherme M. Cunha, MD**[1], **Kathryn J. Fowler, MD**[1], **Michael S. Middleton, MD PhD**[1], **Rohit Loomba, MD**[3,4], **Claude B. Sirlin, MD**[1]

[1]Liver Imaging Group, Department of Radiology, University of California San Diego, La Jolla, California, USA

[2]Computational and Applied Statistic Laboratory, San Diego Supercomputing Center, University of California San Diego, San Diego, California, USA

[3]Division of Epidemiology, Department of Family Medicine and Public Health, University of California San Diego, La Jolla, California, USA

[4]NAFLD Research Center, Division of Gastroenterology, Department of Medicine, University of California San Diego, La Jolla, California, USA

Abstract

Purpose: To estimate parameters determining liver triglyceride composition (TC) using ^{1}H MRS and to assess how TC estimability is affected by proton density fat fraction (PDFF) in adults with nonalcoholic fatty liver disease (NAFLD).

Material and Methods—In this prospective single-site study, 199 adults with known or suspected NAFLD in whom other causes of liver disease were excluded underwent two ^{1}H MRS STimulated Echo Acquisition Method (STEAM) sequences at 3T. A respiratory-gated water-suppressed free breathing sequence (TE 10 ms, 16 signal averages) was used to assess triglyceride composition in terms of number of double bonds (ndb) and methylene-interrupted double bonds (nmidb), and a single breath-hold long-TR, multi-TE sequence (TR 3500 ms) which acquired 5 single average spectra over TE 10–30 ms was used to estimate liver PDFF. Ndb and nmidb estimability was qualitatively assessed for each case and summarized descriptively. Consistency of ndb and nmidb estimation was examined using ROC analysis. Relationship between ndb and nmidb values and PDFF was presented graphically. Quality-of-fit of ndb and nmidb vs. PDFF was evaluated by Pearson-r correlation. A significance level of 0.05 was used.

Results: In 263 ^{1}H MRS exams performed on 199 adult participants, ndb and nmidb were successfully estimated in 7/53 (13.2%) exams with PDFF < 4%, 13/30 (43.3%) exams with PDFF between 4% and 7%, 33/41 (80.5%) exams with PDFF between 7% and 10%, and 124/139 (89.2%) exams with PDFF > 10% (max PDFF 38.1%). Liver TC could be estimated consistently for PDFF > 6.7 %. Both ndb and nmidb decreased with increasing PDFF (ndb = 2.83 - 0.0160·PDFF, r = −0.449 p < 0.0001); nmidb = 0.75 −0.0088·PDFF, r = −0.350, p < 0.0001).

Corresponding Author: Gavin Hamilton PhD, Department of Radiology, University of California San Diego, 9500 Gilman Drive MC 0888, La Jolla, CA 92093-0888, USA, Tel: 858-246-2194, ghamilton@ucsd.edu.

Conclusion: In a cohort of adults with known or suspected NAFLD, liver triglyceride composition becomes more saturated as PDFF increases.

Graphical Abstract

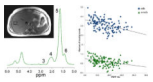

Adults with known or suspected NAFLD underwent two liver ^{1}H MRS STEAM sequences at 3T to investigate how triglyceride composition varies with proton density fat fraction (PDFF). A respiratory-gated water-suppressed sequence was used to characterize liver triglyceride composition in terms of number of −CH=CH− and −CH=CH−CH_2−CH=CH− bonds and a long-TR, multi-TE sequence was used to estimate liver PDFF. ^{1}H MRS indicates that liver triglyceride composition becomes more saturated with increasing PDFF in adults with NAFLD.

Keywords

Magnetic Resonance Spectroscopy; Triglyceride Composition; Fatty Acids; NAFLD; NASH; PDFF; Hepatic Triglyceride Saturation

INTRODUCTION

Magnetic resonance (MR)-based methods can noninvasively, accurately and precisely estimate liver proton density fat fraction (PDFF), a quantitative imaging biomarker of hepatic steatosis.[1–3] Both MR imaging (MRI)- and MR spectroscopy (MRS)-based estimates of PDFF correlate strongly with histologic hepatic steatosis grade,[4–7] and MRI- and MRS-PDFF agree well with each other.[3,8,9] Although liver fat can be accurately quantified using MR-derived PDFF, the lack of a direct correlation between the amount of liver fat and the development of nonalcoholic steatohepatitis (NASH), the progressive form of nonalcoholic fatty liver disease (NAFLD), may to some extent limit its clinical applications.[10,11] The noninvasive characterization of the mixture of fatty acids in liver triglycerides (i.e., the triglyceride composition [TC]) may potentially help us understand why the majority of patients have simple benign steatosis while a minority develop progressed forms of disease. However, the ability of MR techniques to characterize the composition of fatty acid chains in triglycerides is not well established. *Ex vivo* analysis of biopsy samples have suggested TC may independently affect clinical outcomes such as risk or severity of NASH or Type-2 diabetes.[12–14]

Standard MRI-PDFF techniques are not able to assess TC because they assume a predetermined triglyceride spectrum,[15,16] but specialized MRI and MRS techniques have been developed to allow TC to be characterized in terms of three variables: number of -CH=CH- double bonds per molecule (ndb), number of double bonds separated by a single -CH_2- (nmidb; number of methylene-interrupted double bonds), and fatty-acid chain length (CL) (Table 1).[17–20] However, those studies have focused on fat depots outside the liver (yellow bone marrow, adipose tissue),[18–24] have been acquired in small subject groups,[25,26] or were acquired with sequences designed for estimating MRS-PDFF which cannot accurately assess TC except at the highest PDFF values.[17]

In one study based on MRS, subjects with NAFLD had higher saturation and lower unsaturation indices than that seen in healthy controls.[27] In another study, TC (specifically ndb) was indirectly assessed in a large adult population in which liver PDFF bias estimated by confounder-corrected chemical-shift-encoded MRI was studied.[28] To explain the observed changes in bias with PDFF, that study hypothesized that TC was not fixed, with ndb decreasing as PDFF increased,[28] but that hypothesis was not directly tested. Thus, there is a need to determine whether the main parameters characterizing TC (i.e., ndb and nmidb) are correlated with PDFF. Correlation of liver TC with PDFF may act as a confounder when trying to compare liver TC in NASH and non-NASH subjects and if liver TC correlates very strongly with PDFF, this may suggest that liver TC, like PDFF, may not be a good predictor of NASH.

To address these issues, in this study we use a ^{1}H MRS water-suppressed, respiratory-gated sequence in a large subject cohort of adults with known or suspected NAFLD to estimate TC, to assess how TC estimability is affected by PDFF and to determine whether ndb and nmidb are correlated with PDFF.

MATERIALS AND METHODS

This was a prospective, single-site study approved by our Institutional Review Board and compliant with the Health Insurance Portability and Accountability Act. Adult human subjects were recruited from clinical NAFLD studies being conducted at our institution. Prospectively recruited subjects either had biopsy-proven NAFLD or were at risk for NAFLD due to family history or obesity. Patients with other causes of liver disease were excluded by the hepatology investigator (RL). Written informed consent was obtained from all subjects. Subjects were scanned between January 2011 and December 2013 and were included in this analysis if both liver MRS-PDFF, and MR spectra to assess TC were acquired.

MRS Acquisition

Subjects were scanned at 3T (GE Signa EXCITE HDxt, GE Healthcare, Waukesha, WI) with an 8-channel torso array coil. Multi-planar localization images were acquired, and a 20 × 20 × 20 mm voxel was selected within the right lobe of the liver, avoiding the liver edges as well as large biliary or vascular structures. To minimize J coupling effects, ^{1}H MR spectra were acquired using the STimulated Echo Acquisition Method (STEAM) sequence which allows a shorter minimum TE than the Point REsolved SpectroScopy (PRESS) sequence, and the mixing time (TM) for the STEAM sequence was fixed at a minimum value of 5 ms.[29]

Two different STEAM acquisitions were acquired for each subject. For PDFF estimation, a long-TR, multi-TE breath-hold acquisition was used,[8,17,30] while for TC estimation a free-breathing sequence with respiratory gating and water suppression was used. Scanning parameters are given in Table 2. All spectra were shimmed during free breathing. There was no water suppression, and spatial saturation bands around the voxel were disabled to ensure a uniform spectral response across the frequency range of interest.

For PDFF estimation, following a single pre-acquisition excitation, TR 3500 ms single average spectra at TE 10, 15, 20, 25 and 30 ms were acquired in a single 21 s breath-hold. This sequence was chosen as it is regarded as the standard for PDFF estimation.[3,9] For the ndb- and nmidb-estimation sequence to assess liver TC, accurate determination of the area of the individual fat peaks in the range 0–3 ppm (peaks 3, 4, 5 and 6) is required (Table 1). This is challenging for peak 3 at 2.75 ppm, a marker of polyunsaturated triglyceride. This peak is smaller than the other fat peaks, and cannot be accurately determined using a breath-held sequence except at the highest PDFF values.[17] Thus, a non-breath-hold sequence with respiratory gating and water suppression (16 signal averages, approx. 2 min acquisition) was used at a single TE (10 ms) to maximize signal-to-noise ratio (SNR). The T1 relaxation times of the fat peaks are short enough (~400–800 ms) such that variation in TR due to normal respiration (TR 2.5~6 s) will not introduce T1 bias.[18,31,32] Similarly the T2 relaxation times of all the fat peaks (~50–100 ms) are long enough such that the short TE (10 ms) used here is independent of subject T2 variability.[29,31,32]

MRS Analysis

Identical prior-knowledge-based analysis was used to fit all spectra from both sequences using an approach previously defined.[31] Rather than analyze spectra from each of the eight elements in the abdomen coil, spectra from the individual channels were combined using singular value decomposition, so there was only one spectrum per TE to analyze.[33] A single experienced observer (GH) analyzed the spectra using prior knowledge in the Advanced Method for Accurate, Robust and Efficient Spectral fitting (AMARES) algorithm[34] included in the Magnetic Resonance User Interface (MRUI) software package.[35] No post-processing, such as line-broadening was applied. Each of the peaks were modeled by multiple Gaussian resonances. While the frequency of the fat peaks was fixed relative to the main CH_2 peak at 1.3 ppm (peak 5), the water and fat signals in the 4–6 ppm range were not fixed in frequency.[17,31]

For the long-TR, multi-TE breath-hold acquisition, the T2-corrected peak areas of fat (0-3 ppm) and water (4–6 ppm) were estimated by non-linear least-square fitting that minimized the difference between the observed peak areas and values given by theoretical decay. PDFF was estimated as the ratio of T2-corrected fat signal to the sum of T2-corrected water and fat signals, adjusted for fat included in the ‘water’ peak from a previously established standard liver spectrum.[17]

For the respiratory-gated, water-suppressed acquisition, spectra were visually inspected and judged not to be evaluable, and were excluded from further analysis if TC could not be estimated due to obvious artefact, technical failure (such as failure of water suppression), or inadequate spectral quality. If one or more of the individual (i.e., fat peaks 3, 4, 5 and 6 at 2.75, 2.1, 1.3 and 0.9 ppm respectively) was not distinguishable from background noise the spectrum was classified as an SNR failure, whereas if the fat peaks could not be clearly distinguished from each other but were visible from background noise, the spectrum was classified as having failed due to indistinguishable fat. To remove possible temporal bias in determining whether spectra were evaluable, all spectra were re-inspected within a single week in large batches a year or more after the original analysis were performed, by the same

observer who originally analyzed the spectra. The results of the re-inspections were used to determine spectral evaluability, rather than the assessment made at the time of the original analysis. If the spectrum was judged acceptable, the results from spectral fitting that used the same MRUI-based approach as that used for long-TR, multi-TE spectra were recorded. The areas of fat peaks 3, 4, 5 and 6 were corrected for relaxation effects using T2 values from literature (Table 1).[17]

A description of the MRS method employed to calculate ndb and nmidb has already been published [17,18]. Briefly, the relative area of each peak was found by adding the number of hydrogen nuclei with its associated type of bond in the triglyceride molecule. This gives the relative area of the peaks shown in Table 1. As allowing the CL to vary freely produced unstable ndb and nmidb estimates, CL was fixed at 17.5 to match observed values in previous studies.[17,21] The ndb and nmidb values were calculated by non-linearly minimizing the difference between the estimated areas of the fat peaks 3,4,5 and 6, and that given by the theoretical model.

Statistical Analysis

Study sample characteristics were summarized. The relationship between success rate of TC assessment (i.e., of the success rate of ndb and nmidb estimation) and PDFF was summarized. A receiver operating characteristic (ROC) curve examining the success rate of TC assessment was generated and used to identify the PDFF threshold from the optimal combination of sensitivity and specificity that separated success from failure. Logistic regression was used to examine the relationship between PDFF above the selected threshold and the probability of failure. For comparison of TC and PDFF, if a subject had scans at multiple time points, only the first scan was used as that was the scan most likely to occur without treatment or intervention. A scatterplot of ndb and nmidb values vs. PDFF was generated, and the relationship was examined using linear regression and Pearson's correlation. Ndb and nmidb estimations were modeled as a constant plus linear term in PDFF: $ndb = ndb_0 + ndb_1 \cdot PDFF$ and $nmidb = nmidb_0 + nmidb_1 \cdot PDFF$. The relationship between ndb and nmidb was examined using linear regression and Pearson's correlation. Partial correlation between ndb and nmidb without the PDFF effect was assessed. A significance level of 0.05 was used in all calculations in this analysis.

RESULTS

Two hundred sixty-three MRS exams were performed on 199 adult participants (93 males, mean age at first scan of 49.0 yrs [range 22 to 75 yrs]). Of the participants who underwent multiple scans, 33 were scanned twice, five were scanned three times, and six were scanned five times.

TC could be assessed for 177/263 (67.3 %) of the acquired exams. A successful acquisition and three examples of spectra where TG could not be assessed are shown in Figure 1. The success rate of TC assessment increased with increasing PDFF: ndb and nmidb could be estimated in 7/53 (13.2%) exams with PDFF < 4%, 13/30 (43.3%) exams with PDFF between 4% and 7%, 33/41 (80.5%) exams with PDFF between 7% and 10%, and 124/139 (89.2%) exams with PDFF > 10%. Low SNR was the main cause for rejection of 42 exams

(16.0%), with 31 (11.8%) rejected for indistinguishable fat peaks and 13 (4.9%) rejected for failure of water suppression or other artefact. For PDFF < 4%, low SNR was the prime reason for failure with 38 exams rejected for low SNR, 5 for indistinguishable fat peaks and 3 for artefact. For PDFF > 4% the most common reason for failure was indistinguishable fat peaks with 26 exams rejected for indistinguishable fat peaks, 10 for artefact and 4 for low SNR.

An ROC curve for classifying the success of liver TC assessment is shown in Figure 2. From the Youden Index, the threshold separating success from failure is PDFF = 6.7% which gives a sensitivity of 0.910 (95% CI: 0.857–0.947) and a specificity of 0.721 (95% CI: 0.614–0.812). For PDFF > 6.7% there was no significant relationship between PDFF and TC assessment success rate (coefficient p = 0.29). A scatterplot showing the dependence of success and failure on PDFF is shown in Figure 3, with the threshold for the Youden Index (PDFF 6.7%).

One hundred thirty-eight (69.3%) adult participants had successful TC assessment on their first exam. The relationships between the determinants of TC (ndb and nmidb) in these subjects and PDFF are shown in Figure 4. Both ndb and nmidb decreased with increasing PDFF: ndb = 2.83 - 0.0161·PDFF, r = −0.449 (p < 0.0001) and nmidb = 0.75 – 0.0088·PDFF, r = −0.350 (p < 0.0001).

Ndb and nmidb were highly correlated (nmidb = −0.921 + 0.594·ndb, r = 0.847 p < 0.0001). Partial correlation between ndb and nmidb with the effect of PDFF removed was similarly strong (r=0.823, p < 0.0001).

DISCUSSION

In this study, we confirmed that both measures of liver TC (ndb and nmidb) decreased with increasing PDFF. Further, we found that the ^{1}H MRS TC assessment success rate increased with increasing PDFF, and failure was not significantly associated with PDFF above 6.7%.

Variation in liver TC with PDFF was not observed in previous studies.[12–14] However, those were *ex vivo* studies on small patient cohorts. Our data showed considerable scatter of ndb (and nmidb) compared to PDFF, so it is possible that this/these relationships would have been unapparent for smaller numbers of subjects.

Our data suggest that the correlation of measures of liver TC with PDFF may be confounding comparison of liver TC in NASH and non-NASH groups, as these groups typically have different mean PDFFs. However, the relationship between liver TC and PDFF displays considerable scatter and when comparing ndb and nmidb, PDFF has almost no effect on their relationship suggesting that there are factors other than just PDFF driving the behavior of liver TC.

A previous study using similar MRS techniques also did not detect a change in ndb with PDFF.[17] However, as the authors of that study stressed, they did not use a ^{1}H MRS sequence optimized for assessing TC, rather using a sequence optimized for PDFF estimation. Thus, their data would have been weighted towards values from spectra with higher PDFF values.

Further, as fat peak 3 (at 2.75 ppm) was only evident in their sequence for subjects with PDFF > 30%, the authors assumed that the relative area of this peak compared to other fat peaks was the same for all subjects. Our study suggests that this was an incorrect assumption. This may explain why measures of liver TC assessed in that study (ndb = 1.92, nmidb = 0.32) were most similar to values seen at the highest PDFF values in our study. The low-PDFF TC observed in our study is similar to that assessed in adipose tissue using a similar technique.[18,21]

Chemical-shift-encoded MRI (CSE-MRI) uses a multi-peak spectral fat model to estimate PDFF[17] that has been widely applied for CSE-MRI PDFF estimation both in research and in some commercially available clinical MRI-based techniques. While this standard model differs from our findings, the effect on PDFF estimation of varying the liver spectral model across a range of biological plausible TC values has been examined and found to be minimal.[36] Although the maximum ndb in that study (2.7)[36] was slightly lower than our ndb_0 value of 2.83, that study suggests that the standard model is good enough, and spectral models that account for changing liver TC with PDFF are not required for CSE-MRI PDFF estimation.

A previous study indirectly observed that TC changed with PDFF whilst examining bias in MRI-PDFF measurements.[28] To provide a consistent estimate of PDFF, that study hypothesized that liver triglyceride became more saturated as PDFF increased. That study's estimated value for 0^{th}-order change (ndb_0 = 2.74) is close to our estimated value (ndb_0 = 2.83), and although that study was not able to estimate the 1^{st}-order change rate in ndb with PDFF, that change rate in our study ($nmidb_1 = -0.0160$) was similar to their hypothesized value ($ndb_1 = -0.01$). The prior study was unable to estimate change in nmidb. Another MRI study on volunteers at 7T also observed an increase in saturation with increasing PDFF, but this change did not reach significance due to a small cohort size.[26]

Further fine tuning of the TC-assessment sequence may improve SNR by increasing the voxel size or acquiring MR spectra with more averages. However, larger voxel size will produce poorer shims and wider linewidths, which may adversely affect the ability to differentiate fat peaks from each other, and the SNR increase available at clinically feasible scan times is marginal as SNR is proportional to the square root of the number of averages.

Assessments of spectral evaluability were subjective. For this approach to apply in a wider setting, standardized criteria for evaluability for assessing liver TC will be required and eventually, as with spectral analysis, the evaluability analysis would be automated, removing operator bias.

Although for PDFF > 6.7% the success rate of TC assessment was independent of PDFF, this technique has lower success rates at low, but clinically important PDFF values. For example, thresholds for detecting NAFLD with PDFF in the range 3.4 to 6.9% have been proposed,[37] and so there is interest in achieving a better understanding of PDFF behavior in this range. However, our technique has only a moderate success rate in this range.

Our study is an exploratory study. As such, it did not attempt to adjust the estimated PDFF or assessments of TC for subject demographics, or for the presence of NASH. An MR

imaging study using the same triglyceride model that we used here found that liver triglyceride in NASH subjects was more saturated than in those with simple NAFLD.[19] Future studies are required to examine the importance, if any, of our findings that ndb and nmidb decreased (i.e., that liver triglyceride became more saturated) with increasing PDFF. Although biopsies were collected on some of the subjects in our study, these biopsies were performed for clinical care and thus were not available for assessing TC. Hence, we cannot confirm that the values of ndb and nmidb estimated by ^{1}H MRS reflect the actual TC. Though this technique has previously been verified in phantoms,[17] *in vivo* studies comparing MR estimates of TC with biopsy-derived TC have been limited to adipose tissue[38]. Further studies in liver comparing MRS with biopsy-derived estimates of TC and disease severity are required, as the challenges in estimating TC in liver are greater than those in adipose tissue, and liver studies are required to investigate the clinical applicability of this technique.

In conclusion, we have confirmed in a population of adults with known or suspected NAFLD that liver triglyceride becomes more saturated as PDFF increases, have shown at 3T that the ability of ^{1}H MRS to assess liver TC successfully increased as PDFF increased, and that for PDFF > 6.7%, the success rate of TC assessment was independent of PDFF.

Acknowledgments

Grant Support: NIH grants R01-DK088925, RO1-DK075128 and R56-DK090350

Abbreviations:

AMARES	advanced method for accurate, robust and efficient spectral fitting
CL	fatty-acid chain length
MRUI	Magnetic Resonance User Interface
NAFLD	nonalcoholic fatty liver disease
NASH	nonalcoholic steatohepatitis
ndb	number of double bonds
nmidb	number of methylene-interrupted double bonds
PDFF	proton density fat fraction
PRESS	point resolved spectroscopy
ROC	receiver operating characteristic
STEAM	stimulated echo acquisition method
TC	triglyceride composition

REFERENCES

1. Reeder SB, Cruite I, Hamilton G, Sirlin CB. Quantitative assessment of liver fat with magnetic resonance imaging and spectroscopy. J Magn Reson Imaging 2011;34:729–749. [PubMed: 22025886]
2. Reeder SB, Hu HH, Sirlin CB. Proton Density Fat-Fraction: A Standardized MR-Based Biomarker of Tissue Fat Concentration. J Magn Reson Imaging 2012;36:1011–1014. [PubMed: 22777847]
3. Hernando D, Sharma SD, Aliyari Ghasabeh M, et al. Multisite, multivendor validation of the accuracy and reproducibility of proton-density fat-fraction quantification at 1.5T and 3T using a fat–water phantom. Magn Reson Med 2017;77:1516–1524. [PubMed: 27080068]
4. Permutt Z, Le TA, Peterson MR, et al. Correlation between liver histology and novel magnetic resonance imaging in adult patients with non-alcoholic fatty liver disease - MRI accurately quantifies hepatic steatosis in NAFLD. Aliment Pharmacol Ther 2012;36:22–29. [PubMed: 22554256]
5. Idilman IS, Hatice A, Idilman R, et al. Hepatic Steatosis: Quantification by Proton Density Fat Fraction with MR Imaging versus Liver Biopsy. Radiology 2013;267:767–775. [PubMed: 23382293]
6. Tang A, Desai A, Hamilton G, et al. Accuracy of MR imaging-estimated proton density fat fraction for classification of dichotomized histologic steatosis grades in nonalcoholic fatty liver disease. Radiology 2014;274:416–425. [PubMed: 25247408]
7. Idilman IS, Keskin O, Celik A, et al. A comparison of liver fat content as determined by magnetic resonance imaging-proton density fat fraction and MRS versus liver histology in non-alcoholic fatty liver disease. Acta Radiol 2016;57:271–278. [PubMed: 25855666]
8. Meisamy S, Hines CDG, Hamilton G, et al. Quantification of Hepatic Steatosis with T1-independent, T2*-corrected MR Imaging with Spectral Modeling of Fat: Blinded Comparison with MR Spectroscopy. Radiology 2011;258:767–775. [PubMed: 21248233]
9. Yokoo T, Serai S, Pirasteh A, et al. Linearity, Bias, and Precision of Hepatic Proton Density Fat Fraction Measurements by Using MR Imaging: A Meta-Analysis. Radiology 2018;286:486–498. [PubMed: 28892458]
10. Middleton MS, Heba ER, Hooker CA, et al. Agreement Between Magnetic Resonance Imaging Proton Density Fat Fraction Measurements and Pathologist-Assigned Steatosis Grades of Liver Biopsies From Adults With Nonalcoholic Steatohepatitis. Gastroenterology 2017;153:753–761. [PubMed: 28624576]
11. Bril F, Bard D, Lomonaco R, Lai J, Cusi K. Change in hepatic fat content measured by MRI does not predict treatment-induced histological improvement of steatohepatitis. J Hepatol 2019. doi:10.1016/j.jhep.2019.09.018
12. Araya J, Rodrigo R, Videla LA, et al. Increase in long-chain polyunsaturated fatty acid n−6/n−3 ratio in relation to hepatic steatosis in patients with non-alcoholic fatty liver disease. Clin Sci 2004;106:635–643. [PubMed: 14720121]
13. Puri P, Baillie RA, Wiest MM, et al. A lipidomic analysis of nonalcoholic fatty liver disease. Hepatology 2007;46:1081–1090. [PubMed: 17654743]
14. Arendt BM, Comelli EM, Ma DWL, et al. Altered hepatic gene expression in nonalcoholic fatty liver disease is associated with lower hepatic n-3 and n-6 polyunsaturated fatty acids. Hepatology 2015;61:1565–1578. [PubMed: 25581263]
15. Bydder M, Yokoo T, Hamilton G, et al. Relaxation effects in the quantification of fat using gradient echo imaging. Magn Reson Imaging 2008;26:347–359. [PubMed: 18093781]
16. Yu H, Shimakawa A, McKenzie CA, Brodsky E, Brittain JH, Reeder SB. Multiecho water-fat separation and simultaneous R2* estimation with multifrequency fat spectrum modeling. Magn Reson Med 2008;60:1122–1134. [PubMed: 18956464]
17. Hamilton G, Yokoo T, Bydder M, et al. In vivo characterization of the liver fat 1H MR spectrum. NMR Biomed 2011;24:784–790. [PubMed: 21834002]
18. Hamilton G, Schlein AN, Middleton MS, et al. In vivo triglyceride composition of abdominal adipose tissue measured by ^{1}H MRS at 3T. J Magn Reson Imaging 2017;45:1455–1463. [PubMed: 27571403]

19. Leporq B, Lambert SA, Ronot M, Vilgrain V, Van Beers BE. Quantification of the triglyceride fatty acid composition with 3.0 T MRI. NMR Biomed 2014;27:1211–1221. [PubMed: 25125224]
20. Peterson P, Månsson S. Simultaneous quantification of fat content and fatty acid composition using MR imaging. Magn Reson Med 2013;69:688–697. [PubMed: 22532403]
21. Ren J, Dimitrov I, Sherry AD, Malloy CR. Composition of adipose tissue and marrow fat in humans by ^{1}H NMR at 7 Tesla. J Lipid Res 2008;49:2055–2062. [PubMed: 18509197]
22. Dimitrov IE, Douglas D, Ren J, et al. In vivo determination of human breast fat composition by ^{1}H magnetic resonance spectroscopy at 7 T. Magn Reson Med 2012;67:20–26 [PubMed: 21656551]
23. Bydder M, Girard O, Hamilton G. Mapping the double bonds in triglycerides. Magn Reson Imaging 2011;29:1041–1046. [PubMed: 21868182]
24. Schneider M, Janas G, Lugauer F, et al. Accurate fatty acid composition estimation of adipose tissue in the abdomen based on bipolar multi-echo MRI. Magn Reson Med 2019;81:2330–2346. [PubMed: 30368904]
25. Lundbom J, Hakkarainen A, Söderlund S, Westerbacka J, Lundbom N, Taskinen MR. Long-TE1H MRS suggests that liver fat is more saturated than subcutaneous and visceral fat. NMR Biomed 2011;24:238–245. [PubMed: 20821410]
26. Gajdošík M, Chmelík M, Just-Kukurová I, et al. In vivo relaxation behavior of liver compounds at 7 Tesla, measured by single-voxel proton MR spectroscopy. J Magn Reson Imaging 2014;40:1365–1374. [PubMed: 24222653]
27. Erickson ML, Haus JM, Malin SK, Flask CA, McCullough AJ, Kirwan JP. Non-invasive assessment of hepatic lipid subspecies matched with non-alcoholic fatty liver disease phenotype. Nutr Metab Cardiovasc Dis. 2019;29:1197–1204. [PubMed: 31371265]
28. Bydder M, Hamilton G, de Rochefort L, et al. Sources of systematic error in proton density fat fraction (PDFF) quantification in the liver evaluated from magnitude images with different numbers of echoes. NMR Biomed 2018;31:e3843. doi:10.1002/nbm.3843
29. Hamilton G, Middleton MS, Bydder M, et al. Effect of PRESS and STEAM sequences on magnetic resonance spectroscopic liver fat quantification. J Magn Reson Imaging 2009;30:145–152. [PubMed: 19557733]
30. Yokoo T, Shiehmorteza M, Hamilton G, et al. Estimation of Hepatic Proton-Density Fat Fraction by Using MR Imaging at 3.0 T. Radiology 2011;258:749–759. [PubMed: 21212366]
31. Hamilton G, Middleton MS, Hooker JC, et al. In vivo breath-hold ^{1}H MRS simultaneous estimation of liver proton density fat fraction, and T1 and T2 of water and fat, with a multi-TR, multi-TE sequence. J Magn Reson Imaging 2015;42:1538–1543. [PubMed: 26114603]
32. Hamilton G, Smith DL, Bydder M, Nayak KS, Hu HH. MR properties of brown and white adipose tissues. J Magn Reson Imaging 2011;34:468–473. [PubMed: 21780237]
33. Bydder M, Hamilton G, Yokoo T, Sirlin CB. Optimal phased-array combination for spectroscopy. Magn Reson Imaging 2008;26:847–850. [PubMed: 18486392]
34. Vanhamme L, van den Boogaart A, Van Huffel S. Improved Method for Accurate and Efficient Quantification of MRS Data with Use of Prior Knowledge. J Magn Reson 1997;129:35–43. [PubMed: 9405214]
35. Naressi A, Couturier C, Devos JM, et al. Java-based graphical user interface for the MRUI quantitation package. Magn Reson Mater Physics, Biol Med 2001;12:141–152.
36. Hong CW, Mamidipalli A, Hooker JC, et al. MRI proton density fat fraction is robust across the biologically plausible range of triglyceride spectra in adults with nonalcoholic steatohepatitis. J Magn Reson Imaging 2018;47:995–1002. [PubMed: 28851124]
37. Qu Y, Li M, Hamilton G, Zhang YN, Song B. Diagnostic accuracy of hepatic proton density fat fraction measured by magnetic resonance imaging for the evaluation of liver steatosis with histology as reference standard: a meta-analysis. Eur Radiol 2019;29:5180–5189. [PubMed: 30877459]
38. Nemeth A, Segrestin B, Leporq B, et al. 3D Chemical Shift-Encoded MRI for Volume and Composition Quantification of Abdominal Adipose Tissue During an Overfeeding Protocol in Healthy Volunteers. J Magn Reson Imaging 2019;49:1587–1599. [PubMed: 30328237]

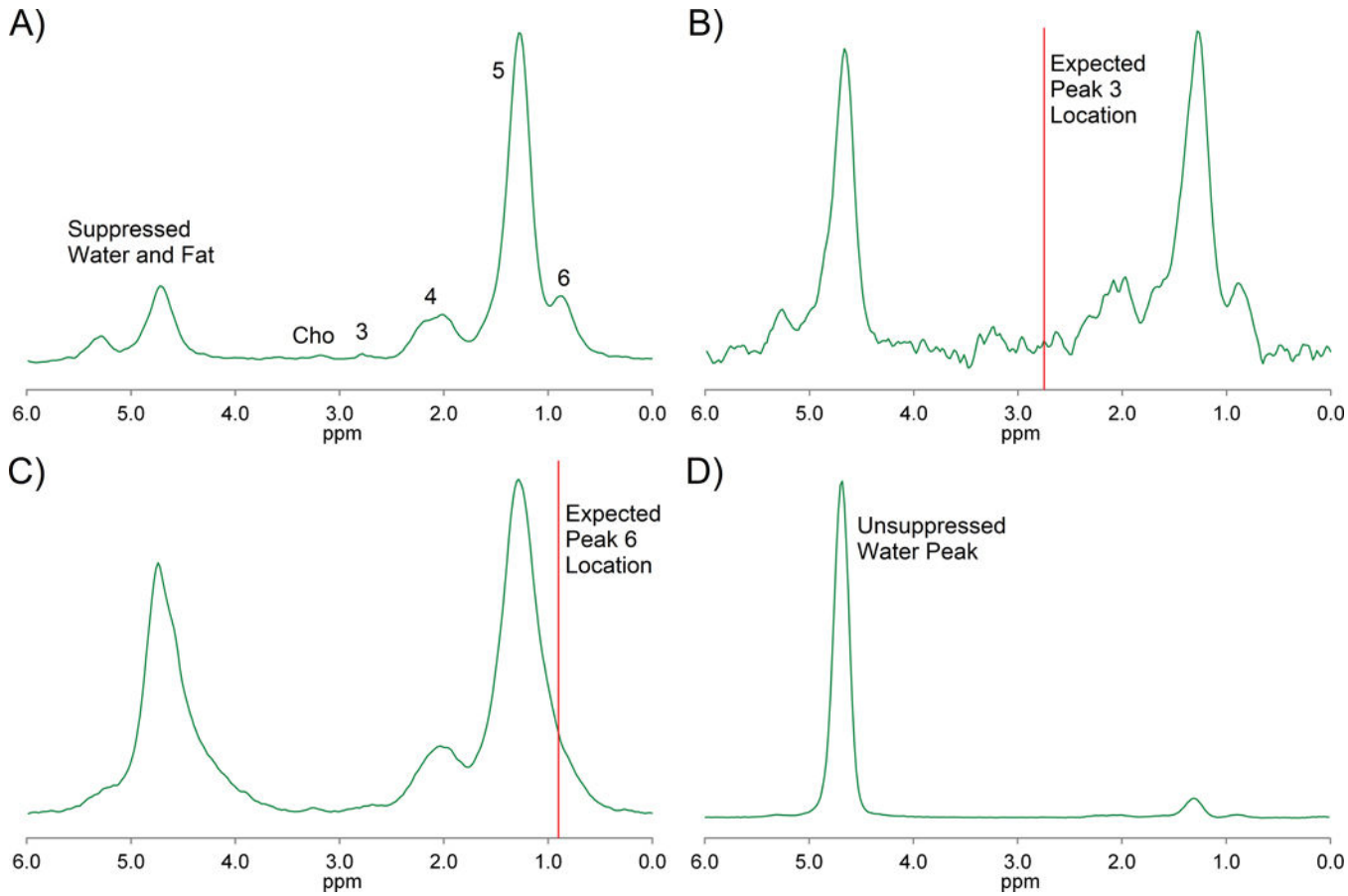

Figure 1.

Four respiratory-gated STEAM, TE 10 ms spectra with 5 Hz Lorentzian line broadening showing successful and inadequate acquisitions: A) successful (PDFF 7.6%); B) inadequate due to low SNR (PDFF 3.4%) with noise between 2.5 and 3.0 ppm obscuring the 2.75 ppm polyunsaturated peak; and C) inadequate due to indistinguishable fat peaks (PDFF 7.7%) obscuring the 0.9 ppm peak and D) inadequate due to failure of water suppression making it challenging to fit the small 2.75 ppm peak (PDFF 7.7%). The fat peak assignments are as in Table 1. Cho - choline containing compounds.

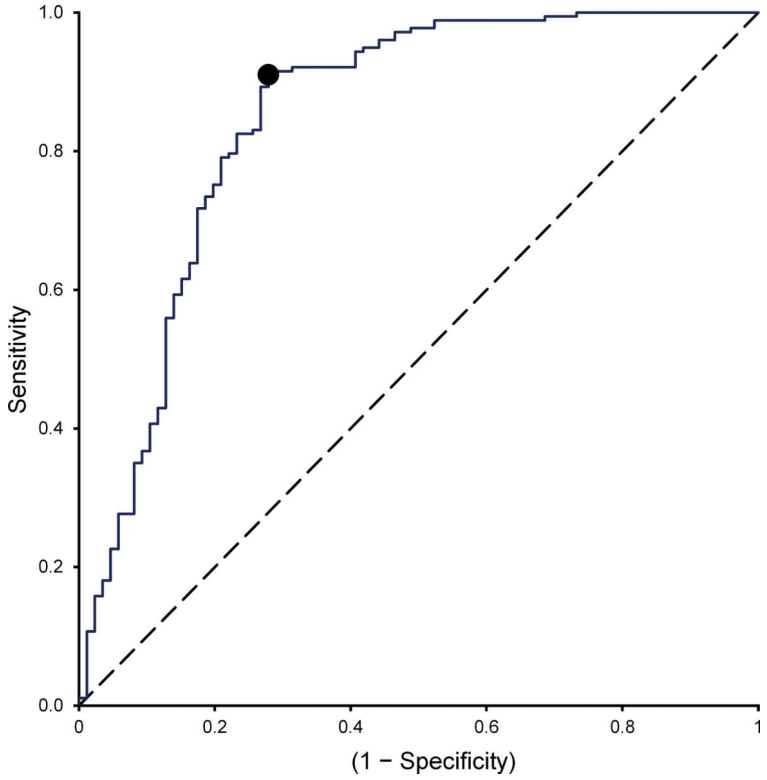

Figure 2.

ROC curve classifying the success rate of liver TC assessment (AUROC = 0.848). The optimal threshold separating success from failure (PDFF = 6.7%) is indicated by a black dot.

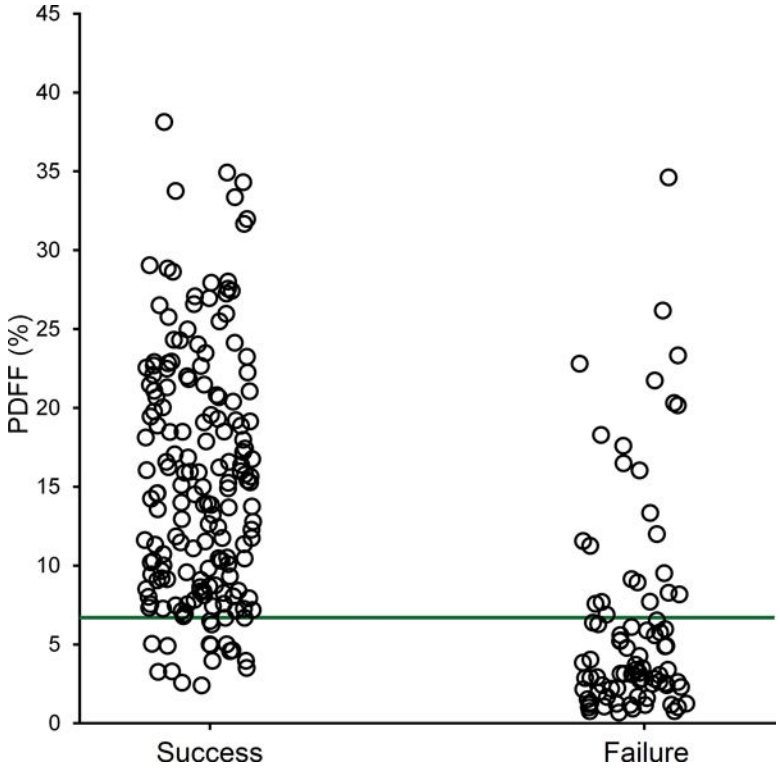

Figure 3.
Scatterplot showing the dependence of success and failure on PDFF with the thresholds for the Youden Index (PDFF 6.7%) shown.

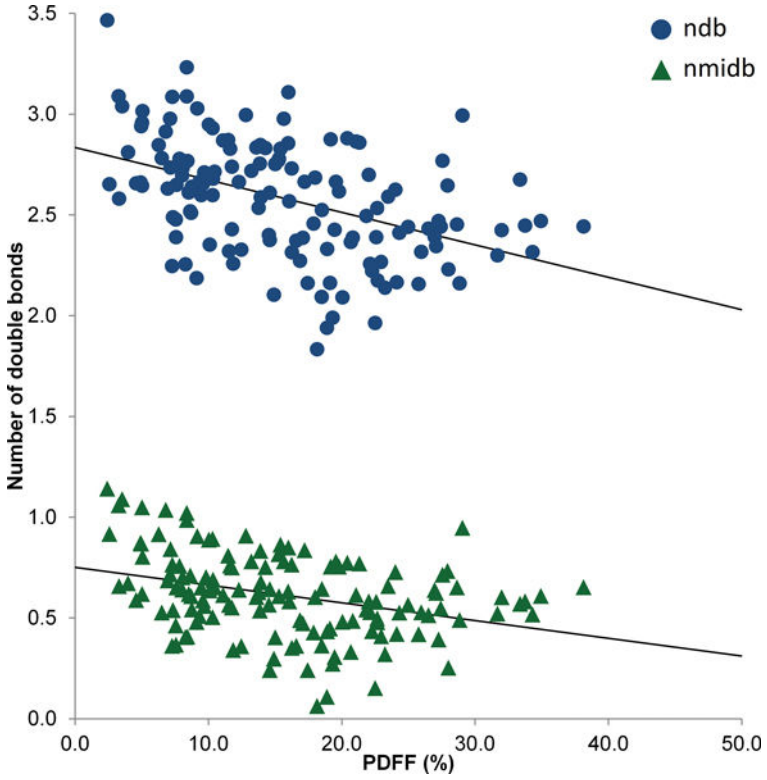

Figure 4.

Comparison of measures of TC assessment (ndb and nmidb) with PDFF. There is correlation between both ndb and nmidb with PDFF, showing liver becoming more saturated as PDFF increases. $ndb_0 = 2.83$ (95% CI 2.74 – 2.93), $ndb_1 = -0.0161$ (95% CI 0.0107 – 0.0215), $r = -0.449$ ($p < 0.0001$) and $nmidb_0 = 0.752$ (95% CI 0.681 – 0.823), $nmidb_1 = -0.0088$ (95% CI −0.0128 – −0.0048), $r = -0.350$ ($p < 0.0001$).

Table 1

Composition of the peaks in the liver ^{1}H MR spectrum with mean T2 from Hamilton et al[17]

Peak	Location	Assignment	Relative Magnitude	In vivo ppm	T2 (ms)
Water (& 1+2)	5.29 ppm	-C**H**=C**H**-	2·ndb	4.7 ppm	23
	5.19 ppm	-C**H**-O-CO-	1		
	4.7 ppm	**H**$_2$O	(Water Signal)		
3	4.20 ppm	-C**H**$_2$-O-CO-	4	2.75 ppm	51
	2.75 ppm	-CH=CH-C**H**$_2$-CH=CH-	2·nmidb		
4	2.24 ppm	-CO-C**H**$_2$-CH$_2$-	6	2.1 ppm	52
	2.02 ppm	-C**H**$_2$-CH=CH-C**H**$_2$-	4·(ndb-nmidb)		
5	1.6 ppm	-CO-CH$_2$-C**H**$_2$-	6	1.3 ppm	62
	1.3 ppm	-(C**H**$_2$)$_n$-	6·(CL-4) - 8·ndb + 2·nmidb		
6	0.90 ppm	-(CH$_2$)$_n$-C**H**$_3$	9	0.9 ppm	83

Table 2

STEAM acquisition parameters for ^{1}H MRS estimation of PDFF and triglyceride composition

	PDFF	Triglyceride composition
TR (ms)	3,500	Respiratory gated
TE (ms)	10, 15, 20, 25, 30	10
TM (ms)	5	5
NSA	1 (per TE)	16
Voxel Size (mm)	20 × 20 × 20	20 × 20 × 20
BW (Hz)	5,000	5,000
Number of points	2,048	2,048
Water suppression	None	CHESS
Scan Time	21 s	~ 2 minutes

Notes: STEAM = stimulated echo acquisition method; MRS = magnetic resonance spectroscopy; PDFF = proton density fat fraction; TR = repetition time; TE = time to echo; TM = mixing time; NSA = number signal averages; BW = bandwidth; Hz = Hertz; CHESS = chemically selective saturation